BIOCHEMISTRY
including biophysical chemistry & molecular biology
Article

Biochemistry **2009,** *48,* 11335–11343 11335
DOI: 10.1021/bi901100b

Reversible Chemical Step and Rate-Limiting Enzyme Regeneration in the Reaction Catalyzed by Formamidopyrimidine-DNA Glycosylase†

Nikita A. Kuznetsov,‡ Dmitry O. Zharkov,‡,§ Vladimir V. Koval,‡,§ Malcolm Buckle,*,∥ and Olga S. Fedorova*,‡,§

‡*Institute of Chemical Biology and Fundamental Medicine, Novosibirsk 630090, Russia,* §*Department of Natural Sciences, Novosibirsk State University, Novosibirsk 630090, Russia, and*∥ *Enzymologie et Cinetique Structurale, Laboratoire de Biotechnologies et Pharmacologie Génétique Appliquées* (*UMR 8113 du CNRS*), *Ecole Normale Superieur de Cachan, 94235 Cachan, France*

Received June 30, 2009; Revised Manuscript Received October 1, 2009

ABSTRACT: Formamidopyrimidine-DNA *N*-glycosylase (Fpg) operates in the base excision repair pathway in bacteria by removing oxidized guanine bases from DNA and can also cleave the nascent or preformed abasic DNA by β,δ-elimination. In this work, we have used the quench-flow technique (i) to show that the kinetics of processing of 7,8-dihydro-8-oxoguanine and abasic site lesions by Fpg from *Escherichia coli* involves a burst phase and a stationary phase, (ii) to establish the reaction kinetic scheme, and (iii) to calculate the rate constants for the reaction steps. A comparison of the quench-flow results with the data from earlier stopped-flow kinetics with tryptophan and 2-aminopurine fluorescence detection reveals that the cleaved product formation is initially reversible; it is followed by conformational changes in the enzyme and DNA molecules that represent the postchemical irreversible rate-limiting steps. We have applied mass spectrometry with electrospray ionization to follow the appearance and disappearance of transient covalent intermediates between Fpg and the substrate DNA. The overall rate-limiting step of the enzymatic reaction seems to be the release of Fpg from its adduct with the 4-oxo-2-pentenal remnant of the deoxyribose moiety formed as a result of DNA strand cleavage by β,δ-elmination.

Reactive oxygen species appear in the cell as byproducts of respiration and may be also generated by environmental factors such as ionizing radiation (*1*). They react with DNA to produce a variety of genotoxic lesions that are considered as possible causative agents in aging and a number of diseases (*2*, *3*). In particular, 7,8-dihydro-8-oxoguanine (oxoG)[1] is one of the most common products of base oxidation in DNA (*4*). It can pair with C, forming a Watson−Crick-type oxoG·C pair, but also easily forms a premutagenic Hoogsteen pair (oxoG·A). In the latter case, replication of an oxoG·A mispair produces a T·A pair, thus leading to a G → T transversion (*5*).

In *Escherichia coli*, a three-enzyme GO system protects the cells from mutagenesis by oxoG (*5*). A central part of this system is formamidopyrimidine-DNA glycosylase (Fpg), which efficiently excises oxoG from DNA when the lesion is paired with C. The glycosidic bond cleavage is initiated by a nucleophilic attack at C1′ by the N-terminal Pro-1 residue, resulting in the formation of a covalent enzyme−DNA Schiff base intermediate, which then rearranges, undergoes sequential elimination of the 3′-phosphate (β-elimination) and the 5′-phosphate (often termed δ-elimination) (Figure 1A) (*6*). The remnant of the deoxyribose moiety (4-oxo-2-pentenal) covalently attached to Pro-1 is hydrolyzed later (*7*). The combined β- and δ-elimination steps are collectively known as the AP lyase activity and also can be catalyzed by Fpg if the substrate is a preformed apurinic/apyrimidinic (AP) site. In all cases, the final reaction products are the excised base, the DNA with a one-nucleotide gap flanked by two phosphates, and a 4-oxo-2-pentenal fragment (*7*−*9*).

The three-dimensional structures of Fpg from several bacterial species in its free form and in different complexes with DNA have been determined (*10*−*17*). DNA binding is accompanied by several drastic conformational changes. The enzyme bends DNA by ∼66°, everts the oxoG residue from DNA to gain access to C1′ of the damaged deoxynucleoside, and inserts amino acid residues Met-73, Arg-108, and Phe-110 into the resulting void in DNA.

Although the mechanism of Fpg action and structures of several complexes in the reaction pathway are known, it is still not clear how Fpg and other DNA glycosylases can robustly select sparse substrate lesions among the vast excess of normal DNA or nonsubstrate lesions. One possibility is that the conformational transitions during substrate binding occur sequentially, with at least some steps structurally optimized for the selection of correct substrates. This model is supported by our previous stopped-flow studies of the Fpg catalytic cycle that used tryptophan (Trp) and 2-aminopurine (2-aPu) as fluorescence reporters (*18*−*20*). This pre-steady-state kinetic analysis of Fpg acting on various DNA substrates and ligands reveals several sequential conformational changes that precede an irreversible step in the reaction pathway. A likely sequence of structural rearrangements leading to preferential recognition of the oxoG·C pair by Fpg has been thus described (*20*).

In addition to Fpg, stopped-flow kinetics with fluorescence detection was used to show that lesion recognition by

†This work was supported in part by grants from the Russian Foundation of Basic Research (07-04-00191, 08-04-00334, 08-04-12211, 08-04-00596, 10-04-00070); Russian Ministry of Education and Science (NS-652.2008.4, MK-987.2008.4, State Contracts 02.740.11.0079 and 02.740.11.5012); the Presidium of the Russian Academy of Sciences (22.14) and the Siberian Branch of the Russian Academy of Sciences (28, 48, 90, 21.22).

*To whom correspondence should be addressed. O.S.F.: e-mail, fedorova@niboch.nsc.ru; phone, +7-383-335-62-47; fax, +7-383-333-36-77. M.B.: e-mail, buckle@lbpa.ens-cachan.fr; phone, +33-1-47407673; fax, +33-1-47407684.

[1]Abbreviations: 2-aPu, 2-aminopurine; AP, apurinic/apyrimidinic; oxoG, 7,8-dihydro-8-oxoguanine; THF, (3-hydroxytetrahydrofuran-2-yl)methyl phosphate.

Published on Web 10/17/2009

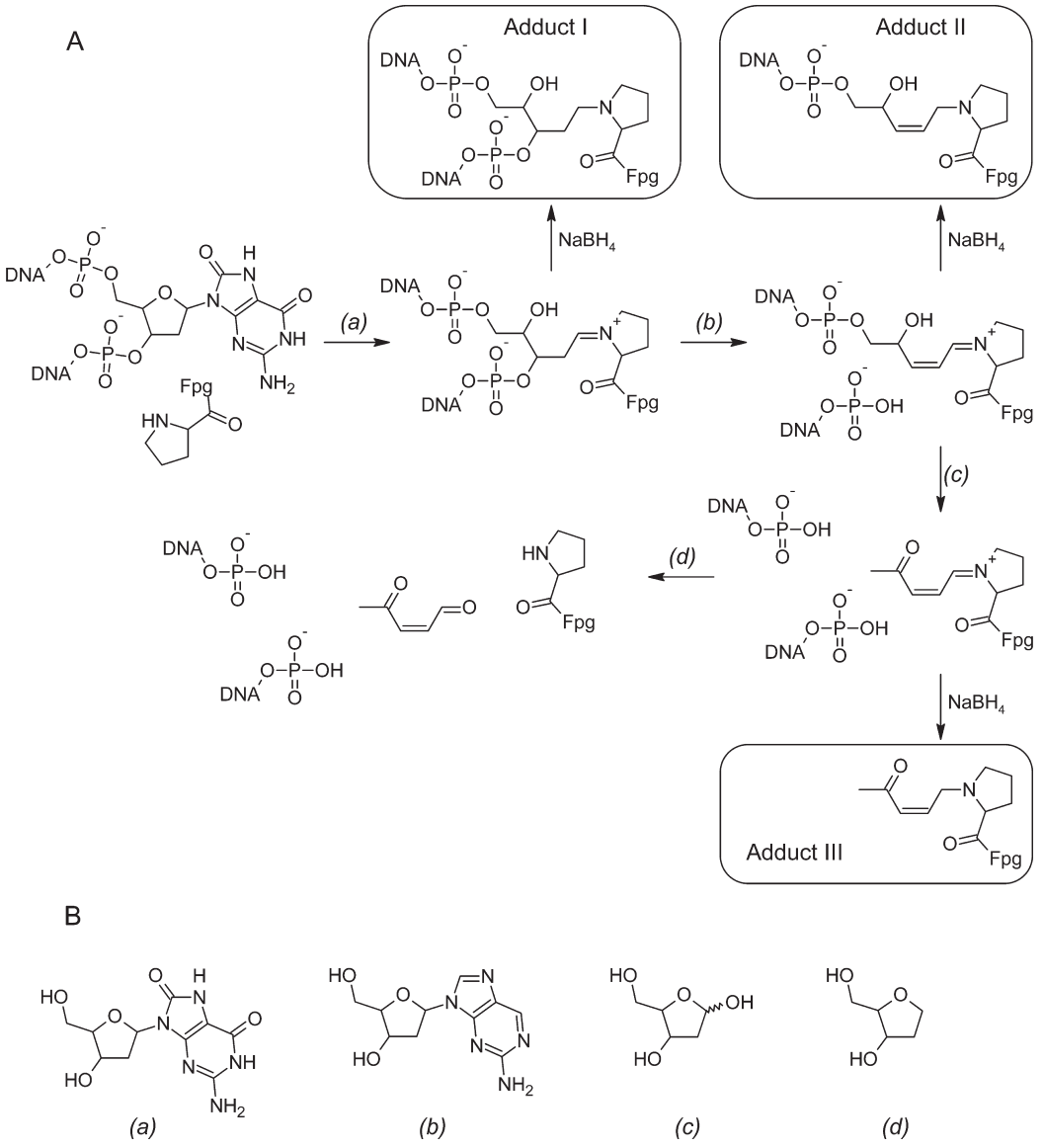

FIGURE 1: (A) Major stages in the reaction catalyzed by Fpg: (a) excision of the damaged base (DNA glycosylase reaction), (b) β-elimination (AP lyase reaction), (c) δ-elimination (AP lyase reaction), and (d) regeneration of the free enzyme. Intermediates leading to different adducts after the reduction with $NaBH_4$ are indicated. (B) Structures of modified deoxynucleosides used in this work: (a) oxoG deoxynucleoside, (b) 2-aPu deoxynucleoside, (c) AP site, and (d) THF.

uracil-DNA glycosylase (*21*), mismatched adenine DNA glycosylase MutY (*22*), and human 8-oxoguanine DNA glycosylase OGG1 (*23*, *24*) involves multiple conformational changes preceding at least one irreversible kinetic step. Importantly, in all these studies, the irreversible kinetic step has been ascribed to the breakage of the N-glycosidic bond of the damaged deoxynucleoside and the following chemical rearrangements. However, in no case except OGG1 is the irreversible step(s) of the reaction accompanied by significant conformational changes; thus, it could not be resolved into fluorescently discernible stages, preventing reliable analysis of the kinetic and contribution of the chemical steps to the specificity of these enzymes. Moreover, recent data concerning human AP endonuclease, an enzyme that, like DNA glycosylases, recognizes and cleaves lesions in DNA, suggest that the chemical steps of the reaction may be reversible, with a later conformational change imparting essential irreversibility to the reaction (*25*).

In this study, we use a microvolume rapid quench technique and mass spectrometry to examine the reactions catalyzed by Fpg and conclude that the initial chemical steps are fast and reversible. The rate of the overall catalytic process is limited by a step after base excision and DNA strand nicking, most likely the regeneration of the enzyme from the covalent complex with the 4-oxo-2-pentenal fragment of the damaged deoxynucleotide.

MATERIALS AND METHODS

Oligodeoxynucleotides and Enzymes. Fpg was purified as described previously (*11*). The fraction of the active enzyme [~90% (Figure S1 of the Supporting Information)] was determined by borohydride trapping (*20*) and taken into account in all experiments. Phosphoramidites of regular and modified deoxynucleosides (Figure 1B) were purchased from Glen Research (Sterling, VA). The oligodeoxynucleotides (Table 1) were synthesized on an ASM-700 synthesizer (BIOSSET) and purified by anion-exchange and reverse-phase chromatography to >98% homogeneity (*19*). AP site-containing substrates were prepared from the oligodeoxynucleotide containing a single deoxyuridine

Table 1: Sequences of Oligodeoxynucleotide Duplexes Used in This Work

	sequence	X	Y
oxoG	5′-CTCTCXCCTTCC-3′		
	3′-GAGAGCGGAAGG-5′	oxoG	
AP	5′-CTCTCXCCTTCC-3′		
	3′-GAGAGCGGAAGG-5′	AP	
THF	5′-CTCTCXYCTTCC-3′		
	3′-GAGAGCCGAAGG-5′	THF	2-aPu

residue by treatment with uracil-DNA glycosylase as described previously (*19*). When necessary, modified oligodeoxynucleosides were labeled at the 5′ end using [γ-^{32}P]ATP (Radioizotop) and T4 polynucleotide kinase (New England Biolabs, Beverly, MA). Oligodeoxynucleotide duplexes were prepared by annealing modified and complementary strands at a 1:1 molar ratio in the reaction buffer. Unless indicated otherwise, all experiments were conducted at 25 °C in buffer containing 50 mM Tris-HCl (pH 7.5), 50 mM KCl, 1 mM EDTA, 1 mM dithiothreitol, and 9% glycerol (v/v). The duplexes used in the experiments are listed in Table 1.

Quench-Flow Measurements. A micro volume rapid quench instrument (RQF-3, KinTek Corp., Austin, TX) was used. Syringes, mixers, and age loops were equilibrated at 25 °C. Urea (7 M) was used as the quench solution. The quenched samples were collected and precipitated via addition of 10 volumes of a 2% $LiClO_4$/acetone solution. The pellets were washed twice with 100 μL of acetone, dried, dissolved in 3 μL of 7 M urea, heated for 2 min at 95 °C, and analyzed by electrophoresis in a 20% polyacrylamide/7 M urea mixture. Gels were dried and exposed to CP-BU X-ray film (Agfa-Gevaert) at −20 °C. The exposition times were calibrated such that the bands corresponding to the separated species were within the linear range of the response of the developed film. The autoradiograms of the gels were scanned and quantified using Gel-Pro Analyzer version 3.0 (Media Cybernetics). Kinetic parameters were obtained by global nonlinear fitting using DynaFit (BioKin, Pullman, WA) (*26*). DynaFit was also used to simulate the reaction and reveal time courses of the appearance and disappearance of the intermediate enzyme·DNA complexes.

Stopped-Flow Measurements. Stopped-flow measurements with fluorescence detection were taken using a model SX.18MV stopped-flow spectrometer (Applied Photophysics). To detect intrinsic Trp fluorescence only, a λ_{ex} of 290 nm was used and a λ_{em} of > 320 nm was followed (Schott filter WG320, Schott). If 2-aPu was present in the ligand, a λ_{ex} of 310 nm was used to excite 2-aPu residues, and their emission was followed at a λ_{em} of > 370 nm (Corion filter LG-370, Newport, Franklin, MA). The dead time of the instrument was 1.4 ms. Each trace shown is the average of four individual experiments. The concentrations of Fpg and the DNA ligand in all experiments were 2 μM.

Trapping of the Schiff Base Intermediate. The cross-linking reaction mixture (10 μL) contained 150 μM oxoG substrate, 100 μM Fpg, 25 mM sodium phosphate (pH 6.8), 100 mM NaCl, and 1 mM EDTA. The reaction was initiated via addition of the enzyme and allowed to proceed at 25 °C for 0−200 s. Freshly dissolved $NaBH_4$ was then added to a final concentration of 100 mM, and the reaction mixture was incubated for 20 min under the same conditions and used for ESI mass spectrometry analysis.

Electrospray Ionization Mass Spectrometry (*ESI-MS*). The samples (3 μL) of the reaction mixtures were assessed on a 5 μm C_{18}, 0.3 mm × 150 mm Zorbax 300SB-C18 column (Agilent Technologies, Santa Clara, CA) with a linear gradient from 0 to 100% solvent B over 20 min at a flow rate of 10 μL/min. Solvent A was 2% acetonitrile with 0.05% formic acid, and solvent B was 50% acetonitrile with 0.05% formic acid. The eluates were analyzed with an ESI-MS mass spectrometer LC/MSD Trap XCT (Agilent Technologies). Mass analysis employed a MS survey scan for 1 s with the mass range of m/z 350−2200. The mass spectrometer was operated in the positive ion spray mode. Nitrogen was used both as the drying gas (4 L/min) and as the nebulization gas (10.0 psi), and the drying temperature was 300 °C.

RESULTS AND DISCUSSION

Rationale. The main objective of this work was to analyze intermediate and product accumulation during DNA cleavage by Fpg and compare these data with the earlier studies (*19*, *20*), where we used detection of fluorescence of Trp and 2-aPu in the stopped-flow mode to analyze conformational changes in Fpg and its DNA ligands or substrates during the reaction. Four and five conformational transitions in the Fpg molecule were revealed by the enzyme's internal Trp fluorescence for AP and oxoG substrate binding, respectively. The analysis of 2-aPu fluorescence provided additional insight into the nature of different steps in the binding model. When the determined structures of Fpg complexed with DNA (*11*−*17*) were taken into account, a comparison of the characteristic times of the appearance and disappearance of different enzyme−substrate intermediates, together with the known decrease in the fluorescence quantum yield of 2-aPu in a less polar environment (*27*), led to a suggestion that the reaction steps in the case of the oxoG substrate correspond to the following events: (1) nonspecific primary encounter, (2) initial recognition with destabilization of DNA around the lesion (possibly with insertion of Phe-110), (3) eversion of the damaged deoxynucleotide from the double helix into the enzyme's active site, (4) filling the resulting void in the double helix with Met-73 and Arg-108, (5) isomerization of the enzyme−substrate complex (observed with oxoG substrates only), (6) chemical steps (cleavage of the glycosidic bond and β- and δ-elimination), and (7) nicked DNA release (*20*).

We have employed the quench-flow technique to analyze the kinetics of cleavage of damaged DNA by Fpg. To be able to analyze not only oxoG substrates but also rather unstable AP substrates, we opted to quench the reaction mixture with urea followed by drying and heating, instead of base or acid quenching. Additionally, the base or acid quenching was undesirable because the reactions catalyzed by Fpg involve several proton movements, and the stability of the reaction intermediates would likely depend on pH in a way that is not straightforward to interpret. Fpg forms a Schiff base covalent intermediate at the first chemical step of the reaction (Figure 1). In addition to being easily hydrolyzable, such imine intermediates undergo β-elimination much faster than their parent aldehydes (*28*−*30*). Aldehydic AP sites are unstable at 95 °C (*31*) and are completely destroyed by drying (*32*); therefore, drying and heating the quenched sample would convert any of the less stable intermediates into free enzyme and nicked DNA that can be detected by gel electrophoresis with autoradiography.

Kinetics of Fpg Unfolding in the Presence of Urea. Prior to approaching the kinetics of Fpg using the quench-flow technique, in which the reaction is terminated by adding a strong

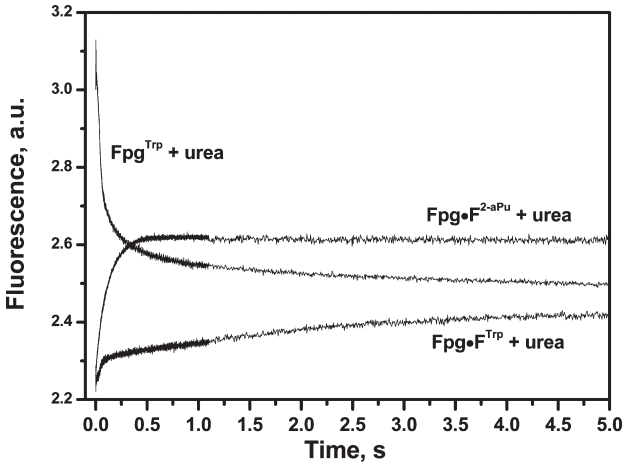

FIGURE 2: Stopped-flow traces of the quenching reaction of 2 μM Fpg without or with 2 μM THF ligand with 7 M urea detected by tryptophan (Fpg^{Trp}, $Fpg\cdot THF^{Trp}$) or 2-aminopurine ($Fpg\cdot THF^{2\text{-}aPu}$) fluorescence.

denaturing agent (urea in our case), we found it was necessary to ensure that the cleavage in the early time range of the reaction truly reflects the enzyme activity at this time point and is not due to inefficient quenching. We have thus first analyzed the kinetics of unfolding of Fpg and the Fpg·THF−ligand complex by 7 M urea using the stopped-flow approach with Trp and 2-aPu fluorescence detection (Figure 2). Under these conditions, a one-step transition of Fpg to a species with a lower fluorescence was observed, presumably reflecting disruption of the enzyme's native structure. The kinetics of denaturation of the Fpg·THF ligand complex also had a single phase of increasing 2-aPu fluorescence, indicating that the enzyme−DNA complex is quickly destroyed. These transitions were both complete by ~260 ms. The Trp fluorescence of the Fpg·THF ligand complex changed at the same time range with two apparent stages, which likely correspond to dissociation of the enzyme−DNA complex and unfolding of the protein. The enzyme likely loses its catalytically competent conformation well before its dissociation or unfolding is complete. Thus, in all further treatment of the quench-flow data, we have added the characteristic time of unfolding ($\tau \sim 130$ ms) to the time points assayed. On the basis of structural evidence, the lesion recognition pocket of Fpg may be destabilized after base excision (*6*) and thus become even more prone to losing its catalytically competent conformation upon addition of urea.

Quench-Flow Measurements of Fpg Kinetics. The results of the quench-flow measurements of cleavage of oxoG- or AP site-containing DNA substrates by Fpg are presented in Figure 3 and Figure S2 of the Supporting Information. All curves showed a fast exponential phase of accumulation of the nicked DNA (burst phase) followed by a linear steady-state phase, characteristic of the overall reaction rate limited by a postincision step. This steady-state phase was not clearly seen in the earlier stopped-flow experiments (*18*−*20*), which were performed mostly under single-turnover conditions. In all cases, we have observed only a single cleaved product band up to the longest reaction times, indicating that the reaction proceeds to complete β,δ-elimination with no kinetically significant accumulation of a β-elimination intermediate.

The minimal kinetic scheme (Scheme 1) that describes the reaction with the burst phase formally indicates that

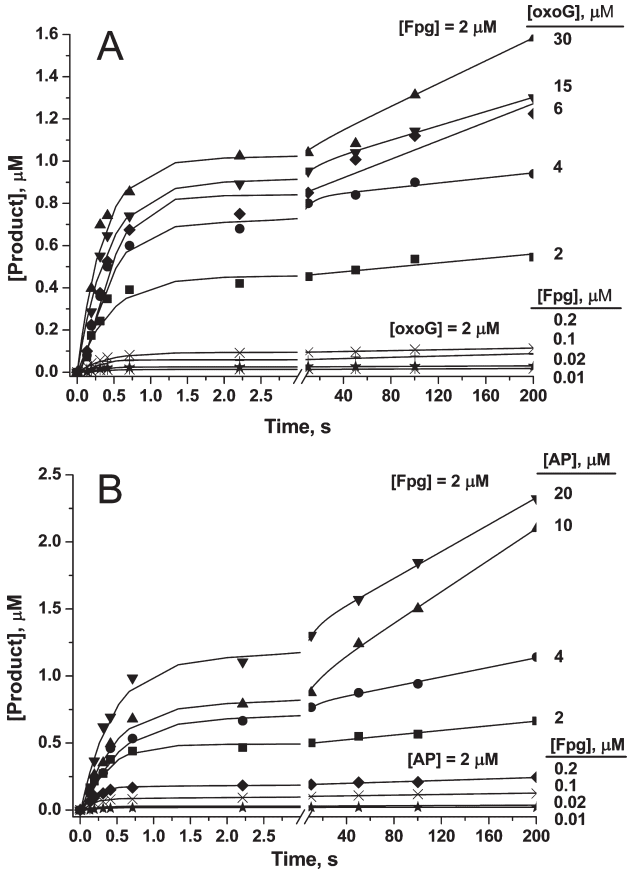

FIGURE 3: Time course of product accumulation ($[P]_{obs}$) during the cleavage of the oxoG substrate (A) and AP substrate (B) by Fpg. For each series of experiments presented here, the concentration of either Fpg or the substrate was fixed at 2 μM, and the concentration of the other component of the reaction was varied as shown next to the fitted curves. The curves result from fitting to Scheme 2.

dissociation of the E·P complex limits the reaction rate (*33*, *34*).

$$E + S \underset{k_{-1}}{\overset{k_1}{\rightleftharpoons}} E\cdot S \xrightarrow{k_2} E\cdot P \xrightarrow{k_3} E + P \qquad \text{(Scheme 1)}$$

This scheme is derived from the assumption that the observed product concentration, $[P]_{obs}$, equals the sum of concentrations of the free cleaved product, [P], and the product in the EP complex, [EP]. It should be noted that the physical meaning of this dissociation process depends on the nature of the EP complex, and that the only requirement for the EP complex in this scheme is that the product in the complex must be identical to the free product P as observed under the conditions of the reaction assay (*33*, *34*). Thus, if the physical meaning is not explicitly specified, the term "product" here and below refers to the species P (either free or in an E·P complex) in the kinetic schemes.

Scheme 1, however, is not the only one that can lead to an appearance of the burst phase. In particular, it can be noted from Figure 3 and Figure S2 of the Supporting Information that the burst amplitudes, obtained by approximation of the linear parts of the total product accumulation curves to zero time, are consistently lower than the respective concentrations of the enzyme. In principle, this could be explained by k_2 and k_3 in Scheme 1 being similar. However, when Scheme 1 was used to calculate the rate constants, the k_3 obtained from the linear parts of the curves was several orders of magnitude less than the k_2

obtained from the burst-phase parts (not shown). Thus, Scheme 1 probably does not describe the quench-flow data adequately. Alternatively, a burst in the product accumulation time course may be observed if the kinetics of the reaction follows the minimal Scheme 2:

$$E + S \underset{k_{-1}}{\overset{k_1}{\rightleftharpoons}} E\cdot S \underset{k_{-2}}{\overset{k_2}{\rightleftharpoons}} E\cdot P \xrightarrow{k_3} E + P \qquad \text{(Scheme 2)}$$

with the product formation being initially reversible. In this case, a decrease in the burst amplitude compared with $[E]_0$ may be caused by the k_{-2} value being comparable with k_2.

The results of fitting of the kinetic data to Scheme 2 are presented in Table 2. It can be seen that while the rate constants of the burst phase, k_2, were similar for both oxoG and AP substrates, the postincision, steady-state rate-determining constant, k_3, was 1.7-fold higher for the AP substrate, indicating that the product release is faster in this case.

Comparison of the Quench-Flow and Stopped-Flow Data. To make a valid comparison of the fluorescently discernible conformational transitions and the time course of cleavage, the quench-flow experiments described above were conducted under exactly the same conditions as the Trp and 2-aPu fluorescence stopped-flow experiments performed previously (*19*, *20*). The product accumulation curves superimposed onto the fluorescence traces are shown in Figure 4. For both oxoG (Figure 4A) and AP substrates (Figure 4B), the burst phase occurred in the same time range, 0.1−1 s, according to the quench-flow data. However, the conformational changes occurring in this time range as revealed by stopped-flow fluorescence data seem to be different in one respect. The burst phase of the product accumulation coincided with a decrease in both Trp and 2-aPu fluorescence in the case of the AP substrate (Figure 4B). These fluorescence stages likely correspond to the plugging of the void formed in DNA by eversion of the damaged deoxynucleotide (*20*). In the case of the oxoG substrate (Figure 4A), the burst phase also corresponds to the decrease in the fluorescence of 2-aPu but the fluorescence of Trp remains approximately steady. The conformational change corresponding to this Trp fluorescence maximum extends from ~0.1 to ~2 s when the substrate contains oxoG but is compressed to 0.1−0.2 s for the AP substrate. As the burst-phase rates were not significantly different for the oxoG and AP substrates, this conformational change obviously does not affect the processes of base excision and/or β-elimination.

In our previous stopped-flow studies (*19*, *20*), we have described the interaction of Fpg with damaged DNA by two kinetic schemes depending of the nature of the fluorophore used to follow the conformational changes in the protein or DNA. When Trp fluorescence was followed, the reaction with oxoG substrate was described by Scheme 3:

$$E + S \underset{k_{-1}}{\overset{k_1}{\rightleftharpoons}} E\cdot S_1 \underset{k_{-2}}{\overset{k_2}{\rightleftharpoons}} E\cdot S_2 \underset{k_{-3}}{\overset{k_3}{\rightleftharpoons}} E\cdot S_3 \underset{k_{-4}}{\overset{k_4}{\rightleftharpoons}} E\cdot S_4 \underset{k_{-5}}{\overset{k_5}{\rightleftharpoons}} E\cdot S_5 \xrightarrow{k_6}$$

$$E\cdot P \overset{K_P}{\rightleftharpoons} E + P \qquad \text{(Scheme 3)}$$

In the case of the AP substrate, the $E\cdot S_5^{Trp}$ complex was absent. When the 2-aPu reporter was used to follow conformational changes in DNA, the reaction was described by Scheme 4:

$$E + S \underset{k_{-1}}{\overset{k_1}{\rightleftharpoons}} E\cdot S_1 \underset{k_{-2}}{\overset{k_2}{\rightleftharpoons}} E\cdot S_2 \xrightarrow{k_3} E\cdot P \overset{K_P}{\rightleftharpoons} E + P \qquad \text{(Scheme 4)}$$

Table 2: Rate Constants for Interactions of Fpg with oxoG and AP Substrates[a]

	oxoG[b]	AP
k_1 (M^{-1} s^{-1})	(640 ± 40) × 10^6	(840 ± 110) × 10^6
k_{-1} (s^{-1})	560 ± 30	290 ± 90
k_2 (s^{-1})	2.5 ± 0.2	2.1 ± 0.1
k_{-2} (s^{-1})	0.3 ± 0.1	0.3 ± 0.1
k_3 (s^{-1})	0.003 ± 0.001	0.005 ± 0.001

[a]Rate constants derived for Scheme 2. [b]Mean ± the standard error of the fit.

The comparison of the characteristic times of the appearance and disappearance of various enzyme·DNA complexes (Figures 5 and 7) shows that the E·S complex inferred from the quench-flow data likely corresponds to the $E\cdot S_1^{Trp}$ and $E\cdot S_2^{Trp}$ complexes and to the $E\cdot S_1^{2\text{-aPu}}$ complex. The beginning of accumulation of the $E\cdot S_3^{Trp}$ complex coincides with the appearance of the $E\cdot P^Q$ complex in both AP and oxoG substrates (the index Q stands for the species inferred from the quench-flow studies). In our earlier analysis (*20*), we suggested that the $E\cdot S_2^{Trp}$ complex corresponds to destabilization of the local DNA structure since at this stage 2-aPu fluorescence also starts to increase, indicating a decrease in the level of stacking of the 2-aPu reporter base adjacent to the damaged base; the $E\cdot S_3^{Trp}$ complex, with the 2-aPu fluorescence still high, was attributed to the eversion of the damaged base out of the DNA helix, whereas the $E\cdot S_4^{Trp}$ complex was ascribed to the plugging step because of the decrease in the 2-aPu fluorescence at this stage. However, it seems from the quench-flow data that the reaction chemistry takes place in the $E\cdot S_3^{Trp}$ complex, and therefore, the damaged deoxynucleoside is fully extrahelical at this step to allow the enzyme to access the C1′ atom, the target of the nucleophilic attack (*11*). Thus, the $E\cdot S_2^{Trp}$ complex would likely correspond to the eversion step, and the base excision and Schiff base formation steps take place before the plugging, which is still attributed to the $E\cdot S_4^{Trp}$ complex. Obviously, the $E\cdot S_4^{Trp}$ and $E\cdot S_5^{Trp}$ complexes (the latter observed in the reaction of cleavage of the oxoG substrate) would also be detected as the $E\cdot P^Q$ complex in the quench-flow experiment since they precede the nicked DNA release step.

The last minimum in the Trp fluorescence traces (arrow in Figure 4A,B) widens with an increase in substrate concentration (*19*) and therefore most likely corresponds to the steady-state phase of the reaction. This conclusion is further corroborated by the observation that in the quench-flow mode this time range coincides with the slow phase of the product accumulation time course (Figure 4A,B). This means that in the steady-state phase the reaction rate is limited not by covalent bond cleavage or formation but by some postincision process. In the case of the oxoG substrate, the slow phase in the quench-flow experiments starts earlier, during the last conformational transition corresponding to the $E\cdot S_5^{Trp}$ complex (Figures 4A and 5C). The apparently lower k_3 value for this substrate (Table 2) can be due to the contribution of this step. The $E\cdot S_5^{Trp}$ complex does not occur with the AP substrate and was earlier attributed to preexcision isomerization of the active site containing the oxoG residue (*19*, *20*). In the new model with the excision occurring in the $E\cdot S_3^{Trp}$ complex, the existence of the $E\cdot S_5^{Trp}$ complex should still be due to the presence of the oxoG residue in the substrate and may represent the release of the excised base from the complex with the enzyme, which, as structural data suggest,

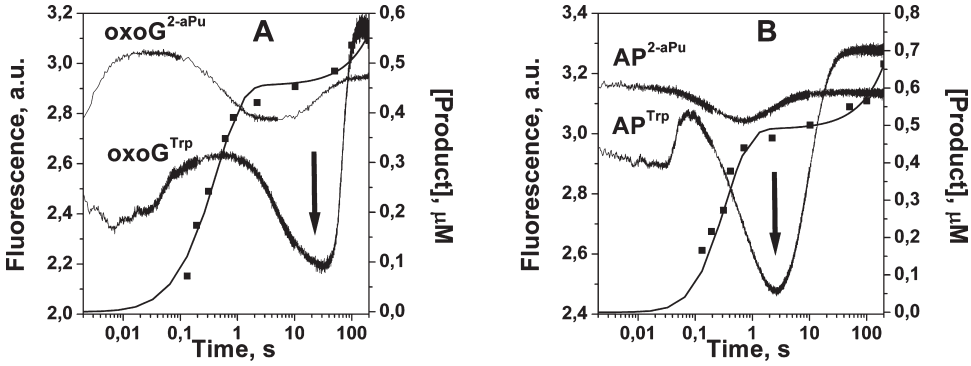

FIGURE 4: Changes in Trp and 2-aPu fluorescence intensity (left axes, data from refs *19* and *20*) and time course of product accumulation (right axes) during interaction of Fpg with oxoG substrate (A) and AP substrate (B). The concentrations of the enzyme and the substrates were 2 μM. Arrows indicate the Trp fluorescence minimum corresponding to the steady-state phase of the reaction.

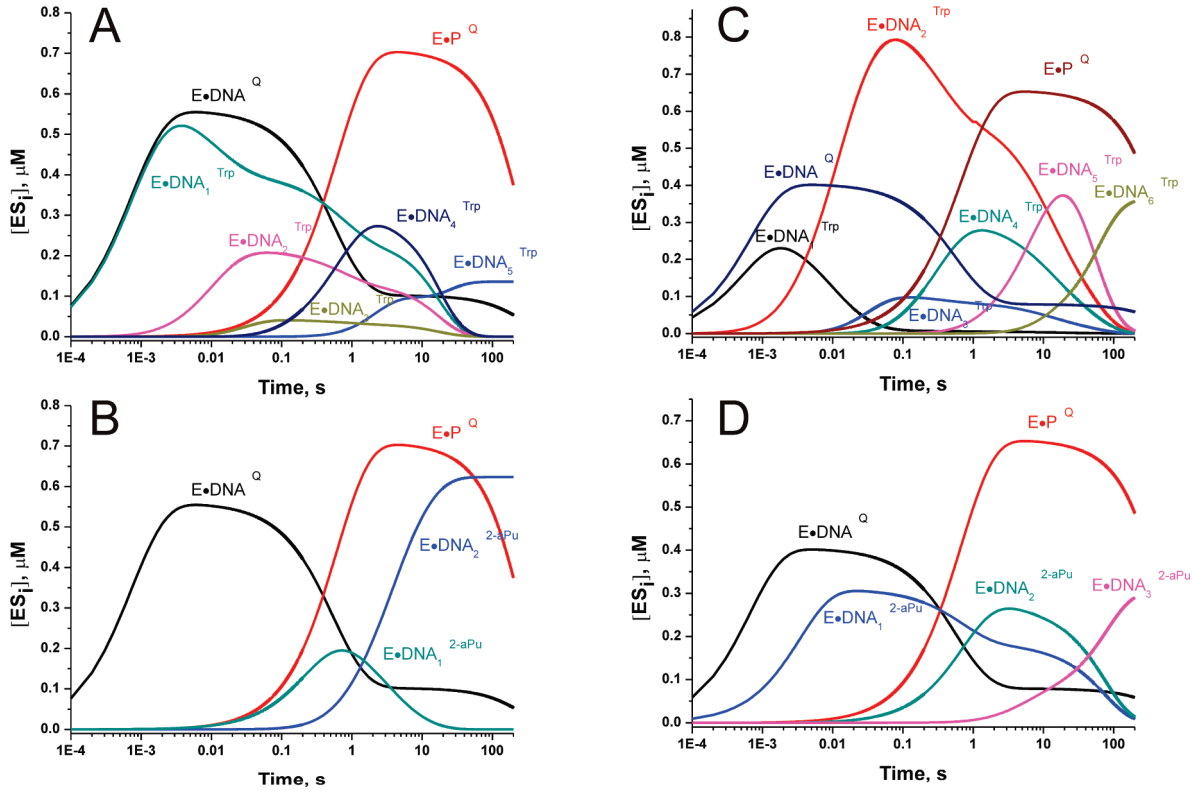

FIGURE 5: Time course of the appearance and disappearance of various enzyme·DNA complexes as revealed by the stopped-flow data (*19*, *20*) with Trp fluorescence detection ($E \cdot S^{Trp}$), 2-aPu fluorescence detection ($E \cdot S^{2\text{-aPu}}$), and quench-flow data ($E \cdot S^{Q}$ and $E \cdot P^{Q}$): (A and B) AP substrate and (C and D) oxoG substrate.

occurs before the nicked DNA product release (*11*) or may be due to postexcision isomerization of the Fpg active site in preparation for release of the base.

The rate-limiting process is not likely to be the dissociation of the enzyme−DNA complex, since this event, the last one in the catalytic cycle, is signaled by the return of Trp and 2-aPu fluorescence to their initial values and occurs later in the reaction than the onset of the step corresponding to the steady state (Figure 4). Thus, the reaction rate appears to be limited by some process occurring after formation of the Schiff base (which takes place during the burst phase) but before the dissociation of the E·P complex. As follows from Scheme 2, the irreversible step in the reaction is also a postincision one. It is possible that the rate-limiting step also makes the reaction essentially irreversible.

Identification of Enzyme−DNA Covalent Complex Intermediates by Mass Spectrometry. Having shown that the observed DNA cleavage likely corresponds to reversible steps of Fpg kinetic scheme, we then turned our attention to the mechanical nature of the irreversible and/or rate-limiting step of the reaction. The mechanism of cleavage of damaged DNA by Fpg involves sequential formation of three enzyme-containing covalent intermediates of the Schiff base type (Figure 1A, reactions a−c), and the nicked product under the conditions we have employed would be observed at any point after the formation of the first of them. Any of the processes after that may be rate-limiting.

The Schiff base intermediates are prone to hydrolysis back to the aldehyde and the amine but can be stabilized by reduction with $NaBH_4$ (Figures 1A and 6A, adducts I−III). To determine the characteristic times of the formation and disappearance of these intermediates, we have used ESI-MS analysis of the reaction mixtures of Fpg and oxoG or AP substrates after their

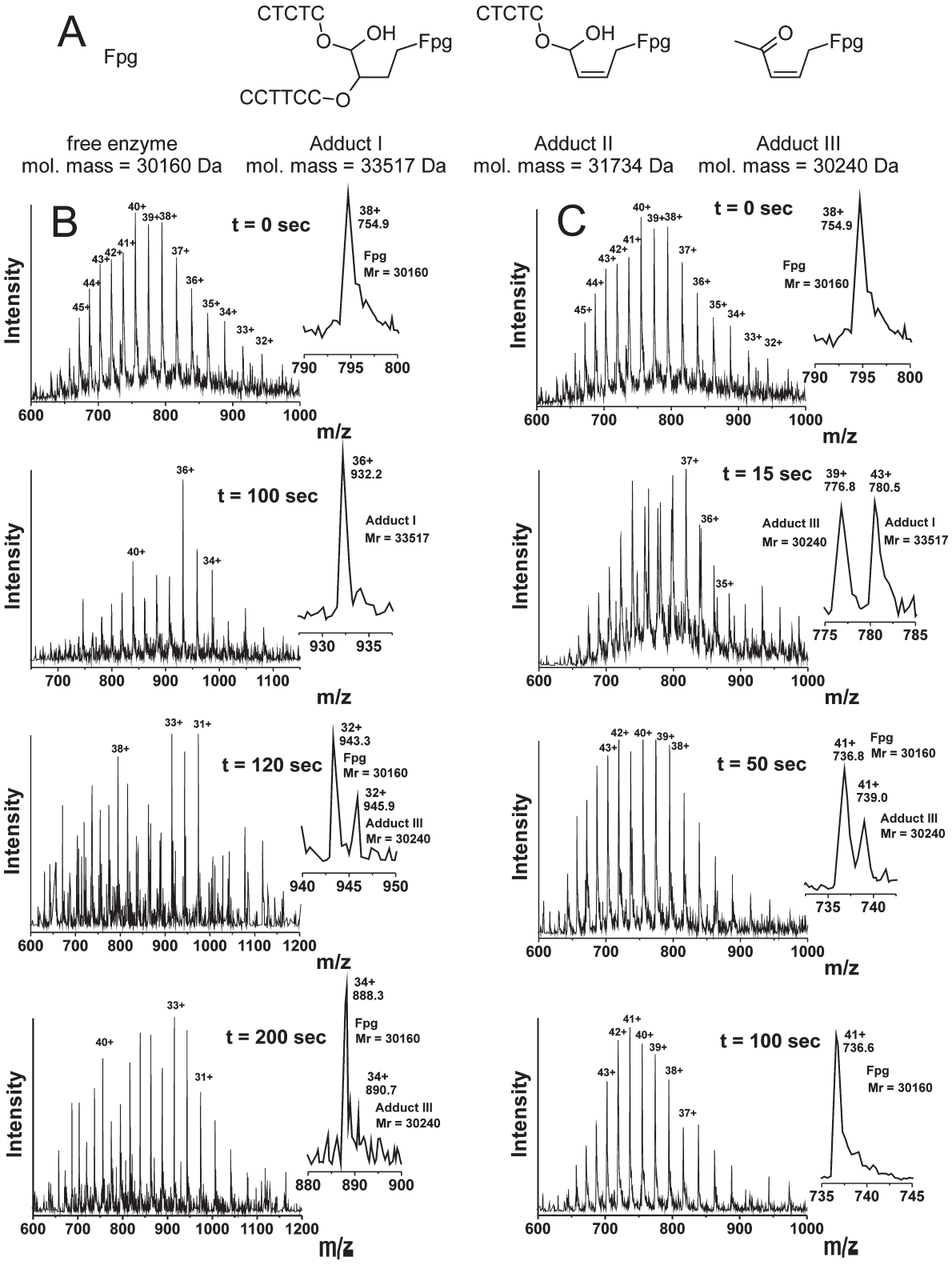

FIGURE 6: (A) Structures and molecular masses of reduced covalent adducts formed during the reaction of Fpg with damaged DNA. (B and C) Positive ion ESI mass spectra of the reaction mixture of Fpg with the oxoG substrate (B) and the AP substrate (C) at different time points. The time shown is the time of the enzymatic reaction and does not include the duration of the $NaBH_4$ treatment.

reduction. In the course of the reaction of Fpg with oxoG or AP substrates under single-turnover conditions, we have added $NaBH_4$ 0−200 s after the initiation of the reaction and subjected the stable cross-linked products to mass spectrometry.

The positive ion ESI mass spectra of the stabilized intermediates of the reaction of oxoG substrate cleavage after $NaBH_4$ reduction are shown in Figure 6B. Despite the addition of a DNA fragment with several negative charges to the protein molecule, the spectra were clean and easy to interpret. At time zero, only a set of single ion peaks with charges from +32 to +46 corresponding to unmodified Fpg (30160 Da) was detected. Early in the reaction (up to 100 s), only the product of reduction of the first covalent complex (adduct I, 33517 Da) was found, again as a series of single peaks. It should be reiterated that, despite the

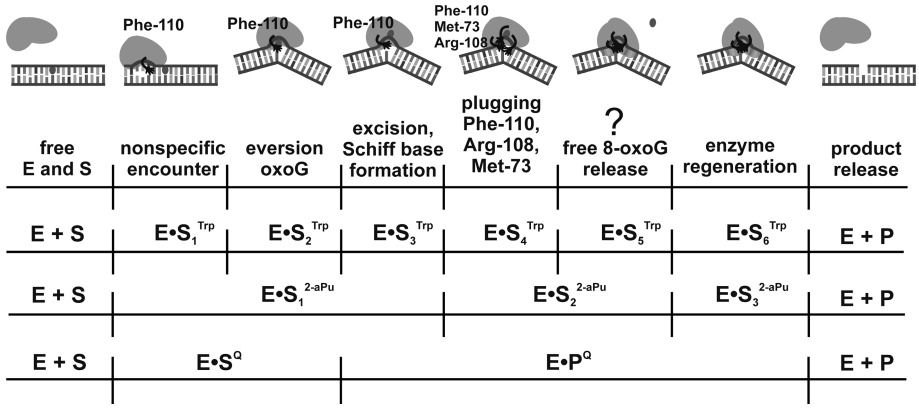

FIGURE 7: Proposed correspondence of different reaction steps and intermediate complexes observed by the stopped-flow technique with Trp fluorescence detection ($E \cdot S^{Trp}$), the stopped-flow technique with 2-aminopurine fluorescence detection ($E \cdot S^{2\text{-}Pu}$), and the quench-flow technique ($E \cdot S^{Q}$).

trapping of the full-length DNA into $NaBH_4$-reduced adduct I, its unstable parent imine would undergo β-elimination and be converted to a nicked product under the conditions of the quench-flow assay. Interestingly, only the product of $NaBH_4$ reduction of adduct III (30240 Da) and free Fpg were identified as soon as 20 s after this (120 s time point), visible as peak doublets (Figure 6B; enlarged peak doublets are shown to the right of the full spectra), whereas no adduct II (31754 Da) was detected at all. The subsequent analysis of the reaction mixture up to 200 s and later (not shown) revealed only free Fpg and decaying peaks of adduct III.

The parallel set of ESI-MS data obtained for the cleavage of the AP substrate by Fpg is presented in Figure 6C. In this case, the reaction proceeded faster, consistent with the literature data on the steady-state kinetics of Fpg (*35*) and the quench-flow data given above (compare k_3 values for both substrates in Table 2). Adducts I and III were both detected already at 15 s; only adduct III and free Fpg were observed at 50 s, and only free Fpg is detected at $\geq$100 s. Therefore, we were able to trap the last covalent complex, leading to adduct III, under single-turnover conditions for the cleavage of both oxoG and AP substrates. As the regeneration of the free enzyme from this complex is required for the steady-state phase of the reaction, the existence of kinetically stable adduct III indicates that the overall reaction in the steady-state mode, reflected by the k_3 constant in Scheme 2, may be limited by the regeneration of the free Fpg from adduct III. Additionally, as indicated above, the release of the excised oxoG base may also contribute to the rate-limiting processes in the case of oxoG substrates, which would explain faster steady-state reaction we have observed with AP-substrate.

CONCLUSION

The mechanisms of lesion recognition and excision by DNA glycosylases, Fpg in particular, involve several conformational changes and chemical steps (*36*). We have employed a quench-flow technique and mass spectrometry to supplement our previous stopped-flow data (*19*, *20*) and place the chemical steps of the reaction into the kinetic scheme established for conformational transitions (Scheme 3, Scheme 4, and Figure 7). In the earlier treatment, it had been assumed that the last, irreversible, rate-limiting step of the reaction corresponds to the combined chemical steps, as is the case with many enzymes (*19*, *20*). However, in this work, we have found that, according to a minimal reaction scheme that adequately fits the quench-flow data (Scheme 2), the products of base excision and/or β,δ-elimination begin to accumulate much earlier in the reaction, during its reversible steps. Although this observation does not represent an unequivocal chemical proof of a reversible covalent bond breakage, it is hardly consistent with the fully irreversible reaction chemistry and strongly suggests that at least some of the processes of Fpg-catalyzed base excision, β-elimination, or δ-elimination are reversible. The overall reaction under the condition of substrate excess seems to be limited by a later, irreversible step. ESI-MS analysis of the reaction intermediate hints that of the covalent reaction intermediates, the Schiff base complex between Fpg and DNA before β-elimination, and the Schiff base complex between Fpg and the five-carbon remnant of the target deoxyribose are the most kinetically stable. Combining this observation with the existence of a late rate-limiting step, we propose enzyme regeneration from the latter covalent adduct as the rate-limiting process. This overall scheme also may be applicable to other glycosylases and AP lyases.

SUPPORTING INFORMATION AVAILABLE

Determination of the concentration of active Fpg (Figure S1), time course of product accumulation during the cleavage of the oxoG substrate (2 μM) by Fpg under the condition of excess substrate (Figure S2A), and dependence of the burst amplitude on Fpg concentration (Figure S2B). This material is available free of charge via the Internet at http://pubs.acs.org.

REFERENCES

1. Halliwell, B., and Gutteridge, J. M. C. (1989) Free Radicals in Biology and Medicine , 2nd ed., Clarendon Press, Oxford, U.K.
2. Wallace, S. S. (2002) Biological consequences of free radical-damaged DNA bases. *Free Radical Biol. Med. 33*, 1–14.
3. Evans, M. D., Dizdaroglu, M., and Cooke, M. S. (2004) Oxidative DNA damage and disease: Induction, repair and significance. *Mutat. Res. 567*, 1–61.
4. ESCODD (European Standards Committee on Oxidative DNA Damage), Gedik, C. M., and Collins, A. (2005) Establishing the background level of base oxidation in human lymphocyte DNA: Results of an interlaboratory validation study. *FASEB J. 19*, 82–84.
5. Grollman, A. P., and Moriya, M. (1993) Mutagenesis by 8-oxoguanine: An enemy within. *Trends Genet. 9*, 246–249.
6. Zharkov, D. O., Shoham, G., and Grollman, A. P. (2003) Structural characterization of the Fpg family of DNA glycosylases. *DNA Repair 2*, 839–862.
7. Bhagwat, M., and Gerlt, J. A. (1996) 3′- and 5′-strand cleavage reactions catalyzed by the Fpg protein from *Escherichia coli* occur via successive β- and δ-elimination mechanisms, respectively. *Biochemistry 35*, 659–665.

8. Bailly, V., Verly, W. G., O'Connor, T., and Laval, J. (1989) Mechanism of DNA strand nicking at apurinic/apyrimidinic sites by *Escherichia coli* [formamidopyrimidine]DNA glycosylase. *Biochem. J. 262*, 581–589.
9. Boiteux, S., O'Connor, T. R., Lederer, F., Gouyette, A., and Laval, J. (1990) Homogeneous *Escherichia coli* FPG protein: A DNA glycosylase which excises imidazole ring-opened purines and nicks DNA at apurinic/apyrimidinic sites. *J. Biol. Chem. 265*, 3916–3922.
10. Sugahara, M., Mikawa, T., Kumasaka, T., Yamamoto, M., Kato, R., Fukuyama, K., Inoue, Y., and Kuramitsu, S. (2000) Crystal structure of a repair enzyme of oxidatively damaged DNA, MutM (Fpg), from an extreme thermophile, *Thermus thermophilus* HB8. *EMBO J. 19*, 3857–3869.
11. Gilboa, R., Zharkov, D. O., Golan, G., Fernandes, A. S., Gerchman, S. E., Matz, E., Kycia, J. H., Grollman, A. P., and Shoham, G. (2002) Structure of formamidopyrimidine-DNA glycosylase covalently complexed to DNA. *J. Biol. Chem. 277*, 19811–19816.
12. Fromme, J. C., and Verdine, G. L. (2002) Structural insights into lesion recognition and repair by the bacterial 8-oxoguanine DNA glycosylase MutM. *Nat. Struct. Biol. 9*, 544–552.
13. Serre, L., Pereira de Jésus, K., Boiteux, S., Zelwer, C., and Castaing, B. (2002) Crystal structure of the *Lactococcus lactis* formamidopyrimidine-DNA glycosylase bound to an abasic site analogue-containing DNA. *EMBO J. 21*, 2854–2865.
14. Fromme, J. C., and Verdine, G. L. (2003) DNA lesion recognition by the bacterial repair enzyme MutM. *J. Biol. Chem. 278*, 51543–51548.
15. Coste, F., Ober, M., Carell, T., Boiteux, S., Zelwer, C., and Castaing, B. (2004) Structural basis for the recognition of the FapydG lesion (2,6-diamino-4-hydroxy-5-formamidopyrimidine) by formamidopyrimidine-DNA glycosylase. *J. Biol. Chem. 279*, 44074–44083.
16. Pereira de Jésus, K., Serre, L., Zelwer, C., and Castaing, B. (2005) Structural insights into abasic site for Fpg specific binding and catalysis: Comparative high-resolution crystallographic studies of Fpg bound to various models of abasic site analogues-containing DNA. *Nucleic Acids Res. 33*, 5936–5944.
17. Banerjee, A., Santos, W. L., and Verdine, G. L. (2006) Structure of a DNA glycosylase searching for lesions. *Science 311*, 1153–1157.
18. Fedorova, O. S., Nevinsky, G. A., Koval, V. V., Ishchenko, A. A., Vasilenko, N. L., and Douglas, K. T. (2002) Stopped-flow kinetic studies of the interaction between *Escherichia coli* Fpg protein and DNA substrates. *Biochemistry 41*, 1520–1528.
19. Koval, V. V., Kuznetsov, N. A., Zharkov, D. O., Ishchenko, A. A., Douglas, K. T., Nevinsky, G. A., and Fedorova, O. S. (2004) Presteady-state kinetics shows differences in processing of various DNA lesions by *Escherichia coli* formamidopyrimidine-DNA glycosylase. *Nucleic Acids Res. 32*, 926–935.
20. Kuznetsov, N. A., Koval, V. V., Zharkov, D. O., Vorobjev, Y. N., Nevinsky, G. A., Douglas, K. T., and Fedorova, O. S. (2007) Presteady-state kinetic study of substrate specificity of *Escherichia coli* formamidopyrimidine-DNA glycosylase. *Biochemistry 46*, 424–435.
21. Wong, I., Lundquist, A. J., Bernards, A. S., and Mosbaugh, D. W. (2002) Presteady-state analysis of a single catalytic turnover by *Escherichia coli* uracil-DNA glycosylase reveals a "pinch-*pull*-push" mechanism. *J. Biol. Chem. 277*, 19424–19432.
22. Bernards, A. S., Miller, J. K., Bao, K. K., and Wong, I. (2002) Flipping duplex DNA inside out: A double base-flipping reaction mechanism by *Escherichia coli* MutY adenine glycosylase. *J. Biol. Chem. 277*, 20960–20964.
23. Kuznetsov, N. A., Koval, V. V., Zharkov, D. O., Nevinsky, G. A., Douglas, K. T., and Fedorova, O. S. (2005) Kinetics of substrate recognition and cleavage by human 8-oxoguanine-DNA glycosylase. *Nucleic Acids Res. 33*, 3919–3931.
24. Kuznetsov, N. A., Koval, V. V., Nevinsky, G. A., Douglas, K. T., Zharkov, D. O., and Fedorova, O. S. (2007) Kinetic conformational analysis of human 8-oxoguanine-DNA glycosylase. *J. Biol. Chem. 282*, 1029–1038.
25. Maher, R. L., and Bloom, L. B. (2007) Pre-steady-state kinetic characterization of the AP endonuclease activity of human AP endonuclease 1. *J. Biol. Chem. 282*, 30577–30585.
26. Kuzmic, P. (1996) Program DYNAFIT for the analysis of enzyme kinetic data: Application to HIV proteinase. *Anal. Biochem. 237*, 260–273.
27. Rachofsky, E. L., Osman, R., and Ross, J. B. A. (2001) Probing structure and dynamics of DNA with 2-aminopurine: Effects of local environment on fluorescence. *Biochemistry 40*, 946–956.
28. Tennant, G. (1979) Imines, nitrones, nitriles, and isocyanides. In Comprehensive Organic Chemistry: The Synthesis and Reactions of Organic Compounds. Vol. 2: Nitrogen Compounds, Carboxylic Acids, Phosphorous Compounds (Sutherland, I. O., Ed.) pp 383−590, Pergamon, New York.
29. Dodson, M. L., Michaels, M. L., and Lloyd, R. S. (1994) Unified catalytic mechanism for DNA glycosylases. *J. Biol. Chem. 269*, 32709–32712.
30. Frey, P. A., and Hegeman, A. D. (2007) Enzymatic Reaction Mechanisms , pp 433−475, Oxford University Press, Oxford, U.K.
31. Sugiyama, H., Fujiwara, T., Ura, A., Tashiro, T., Yamamoto, K., Kawanishi, S., and Saito, I. (1994) Chemistry of thermal degradation of abasic sites in DNA. Mechanistic investigation on thermal DNA strand cleavage of alkylated DNA. *Chem. Res. Toxicol. 7*, 673–683.
32. Shishkina, I. G., and Johnson, F. (2000) A new method for the postsynthetic generation of abasic sites in oligomeric DNA. *Chem. Res. Toxicol. 13*, 907–912.
33. Fierke, C. A., and Hammes, G. G. (1995) Transient kinetic approaches to enzyme mechanisms. *Methods Enzymol. 249*, 3–37.
34. Johnson, K. A., Ed. (2003) Kinetic Analysis of Macromolecules: A Practical Approach , Oxford University Press, Oxford, U.K.
35. Tchou, J., Bodepudi, V., Shibutani, S., Antoshechkin, I., Miller, J., Grollman, A. P., and Johnson, F. (1994) Substrate specificity of Fpg protein: Recognition and cleavage of oxidatively damaged DNA. *J. Biol. Chem. 269*, 15318–15324.
36. Zharkov, D. O., and Grollman, A. P. (2005) The DNA trackwalkers: Principles of lesion search and recognition by DNA glycosylases. *Mutat. Res. 577*, 24–54.